Title

Modeling Non-Backdriving Behavior in an Electromechanical Steering Actuator Using Bond Graphs

Journal

2021 International Conference on Bond Graph Modeling and Simulation, ICBGM 2021, 53(3)

ISSN

07359276

Authors

Loyola, Jonathan
Lee, Kyungbok
Margolis, Donald

Publication Date

2021

Peer reviewed

MODELING NON-BACKDRIVING BEHAVIOR IN AN ELECTROMECHANICAL STEERING ACTUATOR USING BOND GRAPHS

Jonathan Loyola
Department of Mechanical Engineering and Aerospace Engineering,
University of California, Davis, USA. Email:jonloyola@ucdavis.edu

Kyungbok Lee
Steering Engineering Design Team, R&D Division, Hyundai Motor Company,
Hwaseong-si, Gyeonggi-do, 18280, Korea. Email:kblee0606@hyundai.com

Donald L. Margolis
Department of Mechanical Engineering and Aerospace Engineering,
University of California, Davis, USA. Email:dlmargolis@ucdavis.edu

ABSTRACT

In an application of rear-wheel steering for an automobile, an electromechanical steering actuator can be used for positioning the rear wheel's angle. The wheel may experience large forces not only from the motor, but also from the road. However, depending on the configuration of the system, the motor typically cannot be backdriven. If this is not considered in the modeling process, a model of the system may allow backdriving and give erroneous results. This paper explores different methods of implementing the non-backdriving behavior with the aid bond graph modeling. The goal is to compare different ideas of implementation and find an appropriate method for the system presented.

Keywords: Rear-wheel Steering, Vehicle Dynamics, Worm Gear, Non-Backdriving.

1 INTRODUCTION

Rear-wheel steering (RWS) is an automobile topic that has a long history and has gained popularity once again. In part, this is thanks to the update in technology, from hydraulic to electromechanical actuators. This change is an improvement which decreases the packaging size and energy usage. The response of the actuator is improved which can lead to interesting applications such as work from (Loyola and Margolis 2021). Findings from many studies on rear-wheel steering show that RWS can improve the turning capabilities at low speeds and help keep the vehicle stable at high speeds. This technology can be found in many luxury and high performance vehicles offered today.

A low-level controller typically controls the position of the actuator, which in turn controls the position of the tire angle. An example of this is shown in Figure 1. The tires are subject to large forces from the road, which transmit through the tie rods and steering rack. The rack is connected to a transmission which is driven by a motor. The configuration with its major elements is shown in the word bond graph in Figure 2.

The design considered in this paper uses a worm gear with a large gearing ratio for the transmission. Because of this large ratio and the friction in the system, the real system does not allow backdriv-

ICBGM'2021 Nov 8-10, 2021- San Diego, California USA - ©2021 Society for Modeling & Simulation International (SCS)

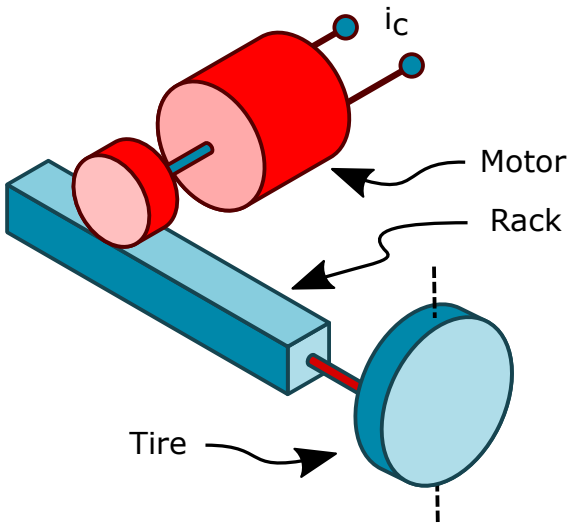

Figure 1: Simplified drawing of a RWS system driven by an electric motor.

Figure 2: Word bond graph of the system.

ing. Backdrivability is described as the ease of a motor to be driven by its attached load when power is removed from the motor. If the motor is non-backdrivable, the motor drives the position of the wheel, but the forces on the wheel cannot drive the motor. However, if a model is constructed without consideration of the non-backdriving properties of the system, the road forces could backdrive the motor, which leads to the motor generating power instead of only discharging power. This can show up in the model, which may not reflect what happens in the real system.

Review of the literature for non-backdriving systems using bond graphs found two authors. The first is (Cheng and Huang 2011), who used an active bond to implement this behavior, shown in Figure 3. The author's bond graph is divided into two parts: Part 1 represents a motor and Part 2 represents a mass-spring system which is later attached to a more complicated model. Connecting Part 1 and Part 2 with an active bond uses the assumption that there is no power exchange between the two systems (or very low power where it is practically negligible). This method would not satisfy our modeling needs, since we cannot make the assumption that there is no back effect from the system. The only assumption is that it cannot be backdriven, which is not equivalent to saying no power is exchanged.

The second author is (Timothy Burke 2000). His thesis sought to create an accurate gear transmission model which was simple enough to incorporate in any bond graph model, taking into account backdrivability. Most literature describes non-backdriving in the static situation, where the gear is locked. He introduces his own definition in the dynamic sense, where he defines non-backdrivable as "A property of an interface between two contacting surfaces across which power can flow in only one direction." This definition omits impulsive forces where the behavior can differ.

The mechanism that prevents backdriving in his model is the combination of stick friction, the lead angle, and the pressure angle between the gears. The model goes on further to include nonlinearities of the gearing systems, such as backlash and Hertzian damping. These nonlinearities are important in his work of studying prosthesis, however, they are not a concern for the modeling in this paper. The author's high fidelity model is implemented later in this paper in order to compare to other proposed methods in this paper. It will serve for validation against the systems proposed here.

This paper builds up the models using the following steps. First, the components of the word bond graph in Figure 2 are modeled with partial bond graphs. Then the components are connected taking into account the causality issues that can occur. Then several proposed methods for the non-backdriving behavior are presented and implemented. Finally, the models are simulated and compared.

2 SUBSYSTEM MODELING

First, the motor is modeled. A simple current driven motor is shown in Figure 4, where R_w represents the winding resistance, J_m is the motor inertia, and T is the transduction coefficient.

The motor drives a pinion which moves a rack. This rack is represented by the partial bond graph

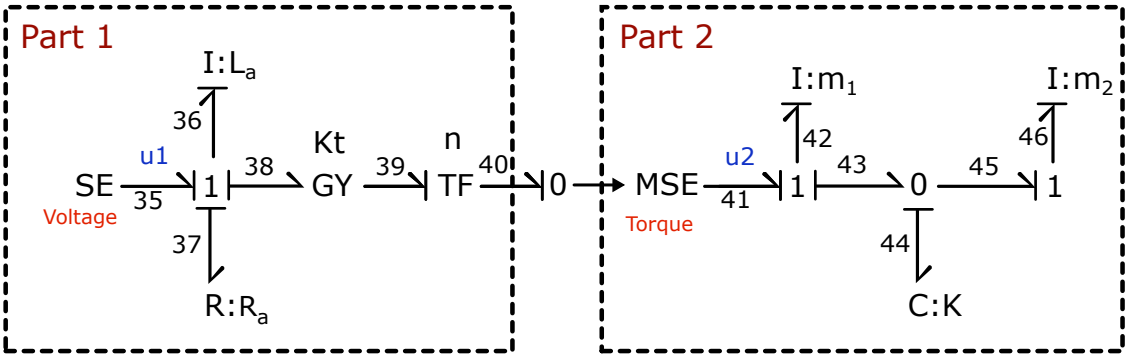

Figure 3: Bond graph with non-backdriving condition (Redrawn from (Cheng and Huang 2011)).

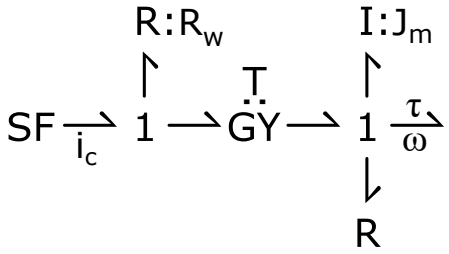

Figure 4: Partial bond graph of a motor.

of Figure 5. In the figure, m_r is the rack mass, and F_r is the force on the rack that is transmitted from the tie rod which is attached to the tire.

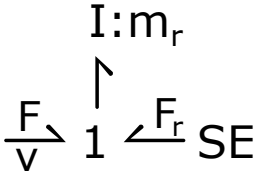

Figure 5: Partial bond graph of a steering rack.

2.1 Gear Modeling

Two different models for the gearing are used in this paper. The first is an ideal rack and pinion with no friction losses. This can be represented by a transformer in the partial bond graph of Figure 6.

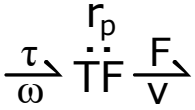

Figure 6: Idealized pinion rack pair.

Attaching this to the partial bond graphs of Figure 5 and Figure 6 yields the following bond graph in Figure 7.

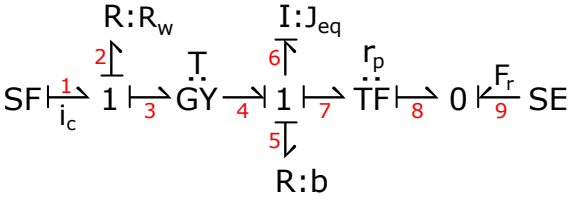

Figure 7: A realization of the word bond graph from Figure 2.

Note that the inertia element associated with the rack mass is omitted. This is due to its effective contribution being very small compared to the moment of inertia of the motor, and its inclusion would result in derivative causality. However, its contribution can be included by combining it with the motor moment of inertia. The inertia parameter can be rewritten as an equivalent inertia parameter where $J_{eq} = J_m + m_r r_p^2$.

The second bond graph model is from (Timothy Burke 2000), shown in Figure 8. This higher fidelity model needs additional parameters to implement, such as the friction between the teeth μ, the pressure angle, ϕ, and the lead angle, λ. Two masses represent the equivalent pinion mass m_p, and the equivalent worm gear mass m_G. The author uses equivalent translational masses which are derived from the moment of inertias. Two nonlinear functions were used in the paper for the capacitance and resistive elements at the top of the bond graph. These represented special damping and backlash properties. Since these are not a con-

cern in this paper, they are replaced by linear relationships.

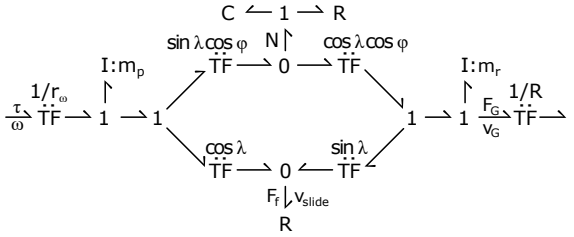

Figure 8: Partial bond graph from (Timothy Burke 2000).

Connecting the subsystems with this model leads to the bond graph in Figure 9.

Some changes were made in order avoid derivative causality. The equivalent mass from m_p is removed. It can be added together with the moment of inertia of the motor.

3 NON-BACKDRIVING CONDITION

As discussed previously, non-backdrivability is described as a property of an interface between two contacting surfaces where power can flow in only one direction. This applies whether the system is at a speed of zero or at a steady state velocity. In order to enforce that the system does not allow any backdriving, the power at the gearing needs to be monitored.

The bond graphs presented above in Figure 7 and Figure 9 shows a motor inertia that sets the flow, which passes through a transformer representing a gearing system or pinion. The loading force downstream propagates back through as an effort. When power at the gearing is negative, this indicates backdriving, where the loading effort is opposite of the flow set by the motor inertia.

In order to prevent backdriving outright, the power should not be allowed to have a negative value. This can be accomplished multiple ways: keeping the effort zero, keeping the flow zero, or keeping both the effort and flow zero. The bond graph in Figure 7 is set up such that the motor side of the transformer sets the flow down to the rack, while the loading on the rack brings back an effort. The most straight forward way would be to not allow that effort due to the loading affect the motion of the motor when the power is negative. These ideas are explored in this section.

3.1 Parameter Modulation

A method to affect the backdriving is modulating parameters of the system depending the sign of the power. Here we explore two elements of the bond graph that could be modulated, a resistance, and an inertia element. The bond graph used to explore these proposed methods is from Figure 7, where the power of **bond 7** is monitored.

3.1.1 Resistance Value

The first parameter that could be changed is a resistance value. The resistance could be modulated according to the following rule:

$$R = \begin{cases} R_{\text{high}}, & \text{if } \tau\omega < 0 \\ R_{\text{low}}, & \text{otherwise} \end{cases}$$

This method won't prevent backdriving outright. It will, however, make the backdriving of the system difficult. The idea is the damping opposes the flow of the motor, attempting to bring the power to zero when its negative. Therefore, referencing the bond graph from Figure 7, we would modulate the resistance associated with **bond 5**. If only viscous damping is assumed, the R modulation would simply be the damping value b.

Monitoring the power at **bond 7** is straightforward. The causality informs us that e_7 depends on the efforts from the rack, and f_7 depends only the motor inertia. An example of how to implement the idea is as follows:

1. Determine the effort and flow at **bond 7** and calculate the power.
2. $$b = \begin{cases} b_{\text{high}}, & \text{if } e_7 f_7 < 0 \\ b_{\text{low}}, & \text{otherwise} \end{cases}$$
3. Proceed with the equations of motion.

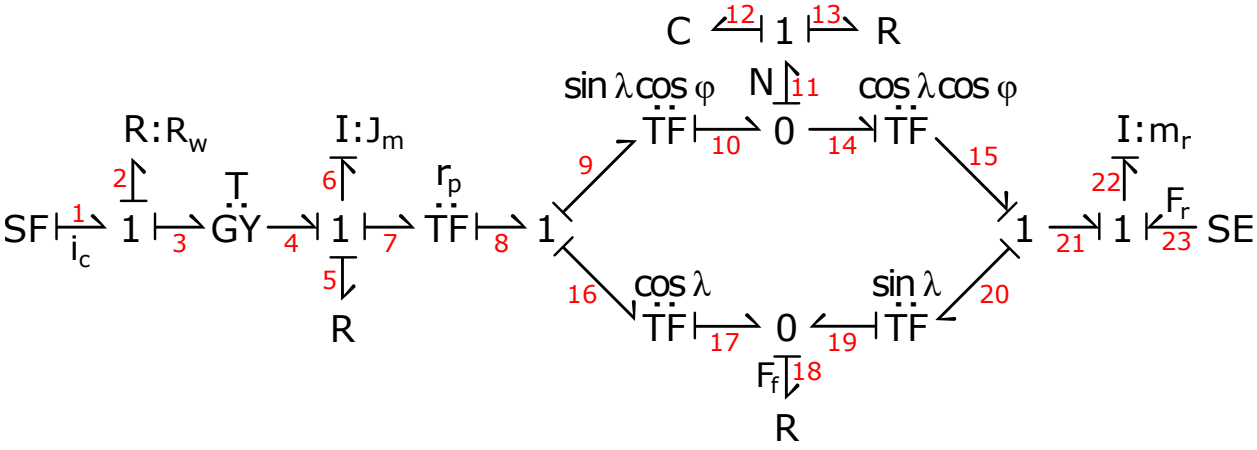

Figure 9: A realization of the word bond graph of Figure 2 using a higher fidelity gear model.

Since the resistance operates on the flow of the motor, extra current may be needed to overcome the resistance when a controller sets the rack position. This concern is explored further in the simulations.

3.1.2 Inertia Value

Another parameter that could be modulated is the value associated with the inertia. The idea would be to make the inertia very large when the power is negative, thus, making it difficult to move and difficult to backdrive. An implementation example is as follows:

1. Determine the effort and flow at **bond 7** and calculate the power.
2. $$I = \begin{cases} I_{\text{high}}, & \text{if } e_7 f_7 < 0 \\ I_{\text{low}}, & \text{otherwise} \end{cases}$$
3. Proceed with the equations of motion.

There are some consequences to this decision. The most important is that the kinetic energy is not conserved when this approach is taken. Care is needed when determining the flow in simulations, and interpreting the results.

In addition, the flow created is directly in the power calculation.

$$\begin{aligned} P &= e_7 f_7 \\ &= (r_p F_r)\left(\frac{p_6}{J_{eq}}\right) \end{aligned}$$

However, in the current configuration of Figure 7, F_r is an effort source in, and J_{eq} is always positive. Whether the inertia is in a high state or low state does not effect the sign of the power.

3.2 Effort Modulation

An alternative method is to not allow any negative power to occur at all. This could involve switching causality and the use of switching junctions. In order to avoid switching causality, a resistance can be added between the connection to the transformer and the motor. This is shown in the following bond graph: Here, **bond 8** would cancel the loading ef-

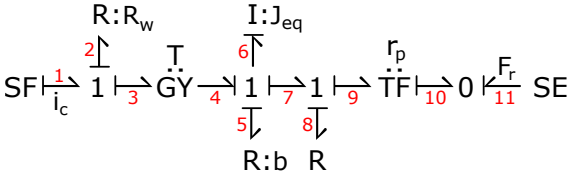

Figure 10: Added resistance for power modulation.

fort from **bond 9** when the power on **bond 9** is negative. Therefore, the power at **bond 7** would be zero. The effort from **bond 8** is simply equal

and opposite. Therefore, the following approach is taken:

1. Determine the power coming through the gearing at **bond 9**.
2. $$\begin{cases} e_8 = -e_9 & \text{if } e_9 f_9 < 0 \\ \text{Do not modulate,} & \text{otherwise} \end{cases}$$
3. Proceed with the equations of motion.

3.3 Advanced Gear Modeling

A higher fideliity gearing system was developed by (Timothy Burke 2000) which requires additional parameters to implement. The criteria for the gear set is developed involving the friction between the gear teeth, the pressure angle, ϕ, and the lead angle, λ. The bond graph is shown in Figure 9. From his work, a simple inequality determines whether the system is backdrivable or not. In order to exhibit the non-backdriving behavior, the following needs to be satisfied:

$$\tan(\lambda)\cos(\phi) < \mu < \frac{1}{\tan(\lambda)\cos(\phi)} \qquad (1)$$

The frictional force from **Bond 18** is due to Coulomb friction, where its implementation uses the Karnopp friction modeling method from (Karnopp 1985).

4 MODELING AND INTEGRATION OF A VEHICLE MODEL

In order to determine how these actuator models behave in a vehicle, they are integrated with a vehicle model. The vehicle model is a classic bicycle model of a vehicle, common in studying the planar dynamics of a vehicle. This is shown in Figure 11.

Figure 12 shows a rack force on the tire though an effective arm, and a road force on the contact patch. This is integrated with the bicycle model, where the list of parameters are given in Table 1.

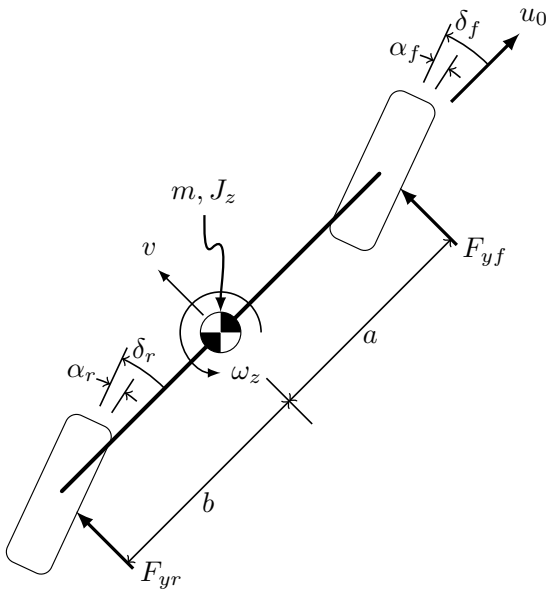

Figure 11: Rear-wheel-steering bicycle model of a car.

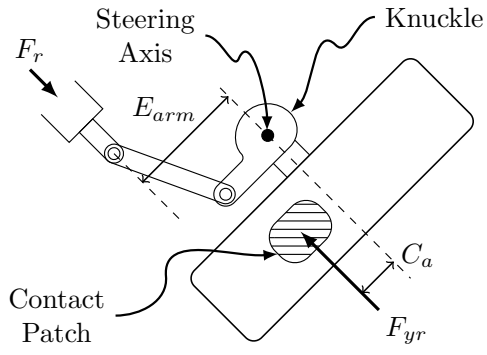

Figure 12: Tire forces at the rear.

Table 1: List of parameters.

Description	Symbol	Units
Mass of vehicle	m	kg
Moment of Inertia	J_z	$kg \cdot m^2$
Length: C.G. to front axle	a	m
Length: C.G. to rear axle	b	m
Cornering stiffness: front	C_f	N/rad
Cornering stiffness: rear	C_r	N/rad
Caster trail	C_a	m
Effective arm	E_{arm}	m
Tire moment of inertia	J_d	$kg \cdot m^2$

The actuator bond graphs show a causality where the rack force effort goes into the system. However, the vehicle model uses a rack force effort into the vehicle system as well. Therefore, a stiff bushing is introduced in order to avoid derivative causality. Figure 13 shows the integration of the steering actuator with a vehicle model.

The stiff bushing uses a capacitance and resistive element. The resistive element is dependent on the motor velocity. This suggests that modulating the inertia can change the sign of the power. The equations are expanded and shown below.

$$\begin{aligned} P &= e_7 f_7 \\ &= (r_p F_r)\left(\frac{p_6}{J_{eq}}\right) \\ &= r_p\left(b_b\left(r_p\frac{p_6}{J_{eq}} - f_{earm}\right) + q_b k_b\right)\left(\frac{p_6}{J_{eq}}\right) \end{aligned}$$

The procedure taken to deal with the implicit issue is to calculate the power every instance assuming the low inertia value. If the power is negative, the high inertia is used instead.

5 SIMULATION

A comparison between the different methods is conducted. However, there will inevitably be difficulties in making fair comparisons as the fidelity of the models include parameters that are not available in every system, especially the higher fidelity gear set.

Six different conditions are compared: a system where non-backdriving is not considered, the resistance modulated system, the inertia modulated system, the effort modulated system, the advanced gearing system, and finally the active bond system.

In order to organize the systems better, the models are labeled as follows:

- Model A: Backdriving not considered
- Model B: Resistance Modulated
- Model C: Inertia Modulated
- Model D: Effort Modulated
- Model E: Advanced Gearing
- Model F: Active Bond

Models A, B, and C use the bond graph from Figure 7, using their respective backdriving methodologies described in previous sections. Model D uses the bond graph from Figure 10, Model E uses the bond graph from Figure 9, and finally Model F uses the bond graph shown in Figure 14.

5.1 Response to Step Loading without a Vehicle

The first test is to check the response of an unpowered motor at rest that is subjected to a step load. This does not use the vehicle model. A source effort is used to feed in the rack force. This is to check how the position of the motor and rack moves and validate the models are working as expected. It is expected that Model D, E, and F would remain at zero, while the other models would allow the rack to move. The simulation consists of a filtered step input of 5000 N pushing on the rack.

The rack response is as expected, shown in Figure 15. Model A, which has a transformer with no losses, displaces the rack at the fastest rate. This is followed by Model B which uses $b_{high} = 10 \times b_{low}$. Increasing the value of b_{high} can further help reduce the rate at which the rack displaces and trend better towards the non-backdriving behavior. However, increasing the value also has effects that are not desirable in the transient, discussed in the next section.

Model C seems to have good results in the first few seconds, where its large inertia slows the rate at

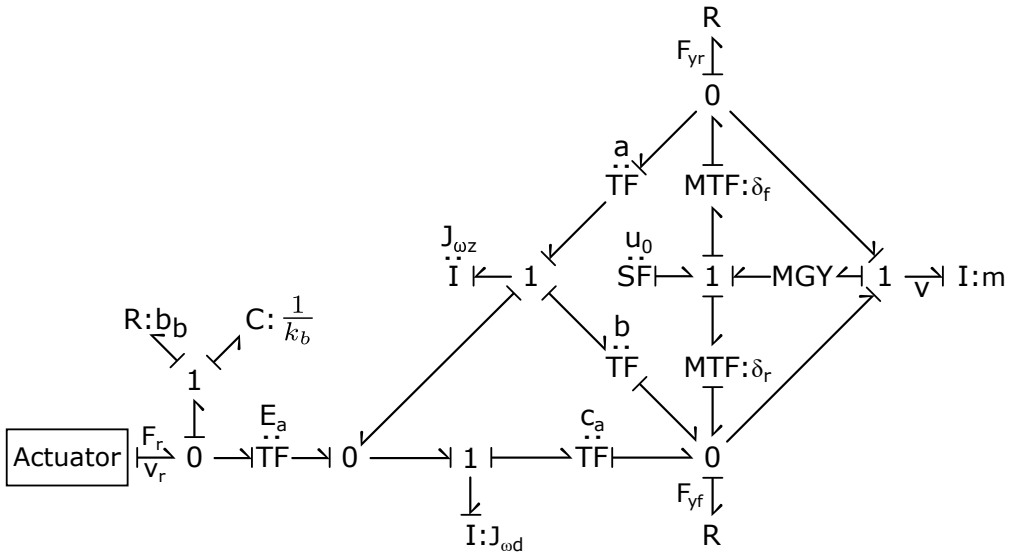

Figure 13: Bond graph of a rear wheel actuator with a bicycle model of a car.

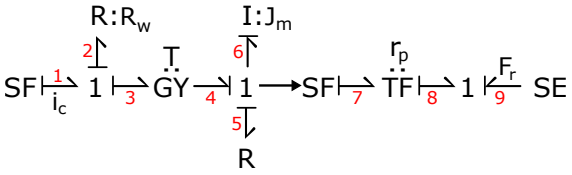

Figure 14: Bond graph of Model F with an active bond.

which the rack moves. In the simulation $I_{high} = 100,000 \times I_{low}$. However like Model A and Model B, the rack continues to displace. All other models stay at zero.

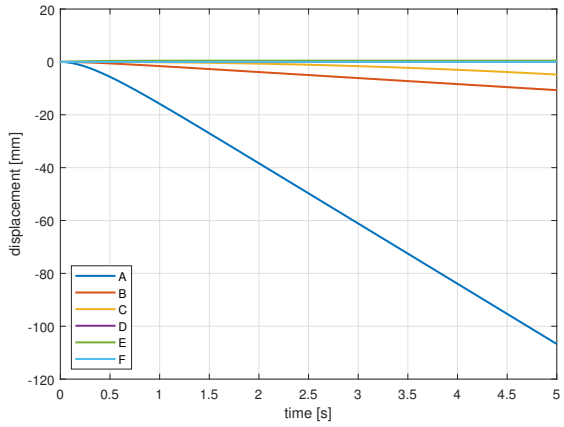

Figure 15: Rack displacement during a rack force step input.

The power can be seen in Figure 16. The plot shows that Model A, B, and C have negative power while the other models stay at zero. These results show that the modeling methods are doing what is expected when the motor is not being driven. The next subsection looks at integrating the actuator model with the vehicle model.

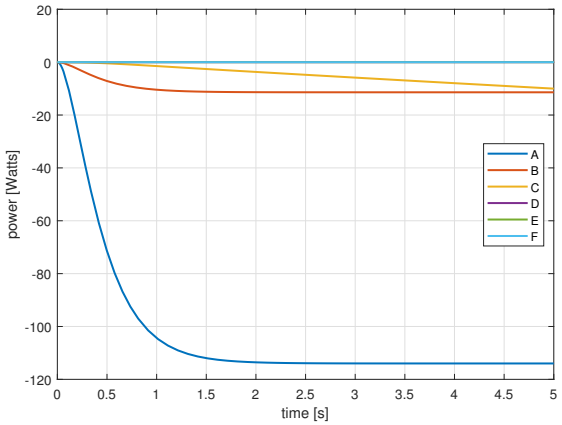

Figure 16: Power at the gearing during a rack force step input.

5.2 Response with a Vehicle Model

All actuator models, Models A-F, are integrated into the vehicle model of Figure 13 and simulated. The input into the system is a sinusoidal tire angle at the front, and the rear is controlled through a PI controller. Conventional rear wheel steering uses the forward speed to schedule how much to

steer the rear according to how much the front is steered. The amount is a ratio of the front wheel, where for these simulations is a ratio of 1:0.2. In the simulations the vehicle is traveling at a constant forward speed of 60 mph.

5.2.1 Sine Input

The steering amplitude of the sinusoidal input is 2° at the front tire, while the frequency is 0.5 Hz. Typical steering input from a driver can range in frequency content up to about 1 Hz. A few cycles of the control response to the sinusoidal input is shown in Figure 17.

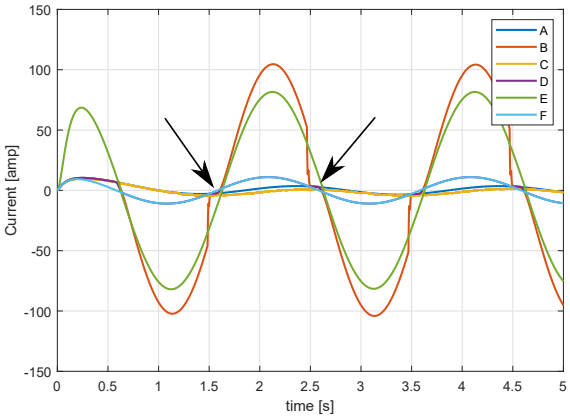

Figure 17: Control response to a sinusoidal front tire input.

The plot of the current shows that Model B and E require the highest amount of current. This is due to Model B increasing the resistance to reduce the backdriving, while Model E uses a high fidelity gear set whose lead angles and pressure angles decrease the efficiency of the system. Model D follows Model F, except at the points indicated by the arrows in the figure. The current for Model B, D, E, and F seem to be in phase which each other except where the arrows point, which indicates that the power might be changing signs.

These points are shown in better detail in Figure 18, where Model D follows Model F for most of the simulation until it follows Model A momentarily indicated by the arrows. These deviations shows moments in the simulation where the power is positive, allowing the force experienced by the vehicle's wheels to propagate back to the motor.

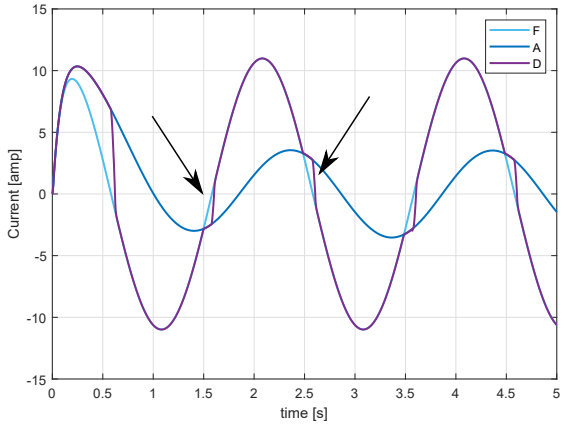

Figure 18: Control response of Models A, D, and F to a sinusoidal front tire input.

This is seen better in Figure 19, where the efforts that would propagate back to the motor from the rack and gearing are shown. Model F is an active bond, so the effort never propagates back. Model A always propagates the effort back to the motor. Model D only propagates back when the power is positive. Therefore, these arrows indicate locations where power is positive.

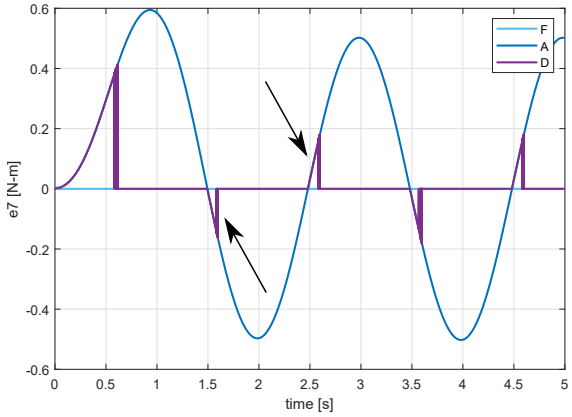

Figure 19: Effort from gearing/rack caused by the road for Models A, D, and F.

The power response in Figure 20 shows that indeed at a second interval starting at 0.5 seconds, the power spikes positive on models A-E. Model C, and D remain at approximately zero power until reaching the location of the arrows. The power remains small for all of the models except for the peaks from Model B and the larger overall power from Model E.

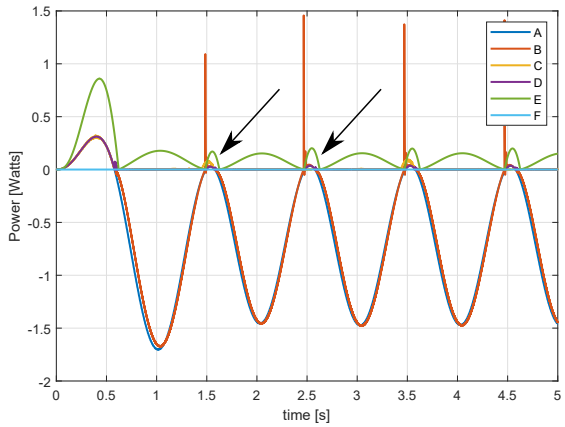

Figure 20: Power at the gearing during a sinusoidal front tire input.

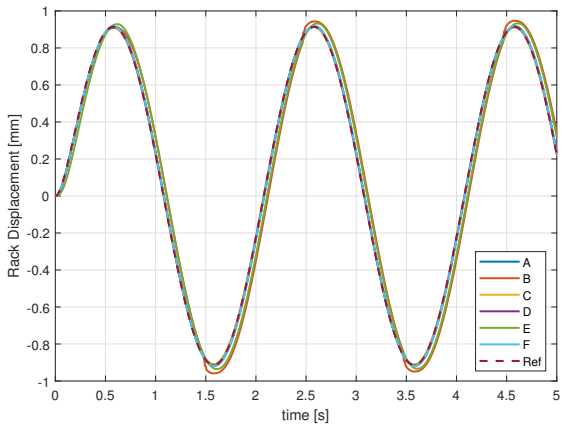

Figure 21: Rack displacement during a sinusoidal front tire input.

As expected, Model A and B allow for negative power in the system. Model C, however, does well keeping the power near zero instead of going negative. Model F is always zero because of the active bond.

Model B uses only 10 times the amount of the nominal resistance value for its b_{high} value. The reasoning behind this choice is increasing the value increases the current and peak in power, which goes against the purpose of trying these different modeling approaches. The outputs of the simulation are deemed excessive and not realistic when the parameter is increased further.

Model C uses a large value for its I_{high} value relative to its nominal value. Depending on how large of a choice is made, the simulation can slow down. Using the ode45 solver from Matlab can give relatively fast results, but large oscillations show up. Using a stiff solver like ode23 can give smoother results, but significantly slows the simulation time.

The rack displacement plot in Figure 21 shows that all the models have good tracking of the reference.

5.2.2 Step Input

In this simulation the driver inputs a filtered step of 2° for the front tire instead of a sinusoid. What would be interesting to look at is the steady state current the models end up with. Figure 22 shows that models A, B, and C all reach the same steady state value for the current necessary to hold the turn. Model D and E uses a smaller value, and finally Model F is 0.

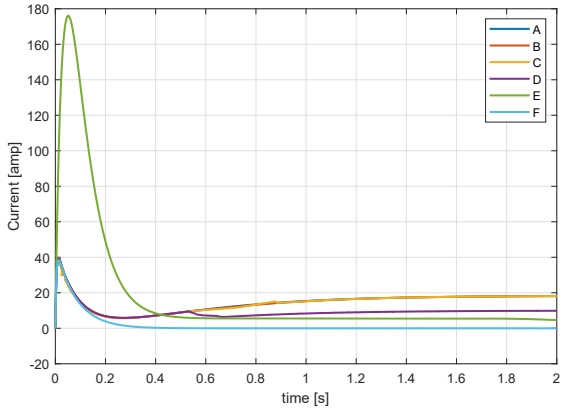

Figure 22: Motor response to a sinusoidal front steering input.

The current for Models A, B, C, D, and F are near identical in the transient for the first 0.1 seconds. Model E produces a much larger transient where the current reaches 170 amps.

The power response is shown in Figure 23. The power for Models A, B, C, and D are near identical for the first 0.5 seconds where the final values are very close to zero. Models A-D all have very small amounts of chattering, while model E smooths out.

The rack displacement plot of Figure 24 shows each model except model E are nearly identical. Model E lags and takes longer to reach its final value.

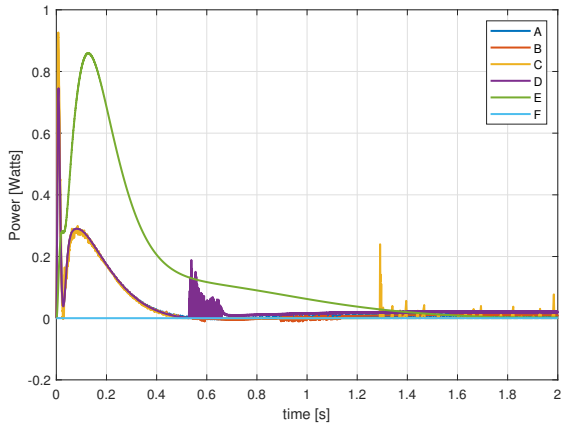

Figure 23: Power at the gearing from a sinusoidal front steering input, and rack position.

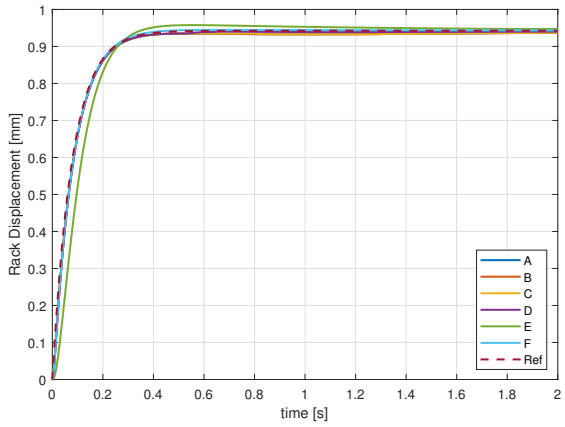

Figure 24: Power at the gearing from a sinusoidal front steering input, and rack position.

6 CONCLUSION

In conclusion, several models were created in order to represent the non-backdriving condition in the gearing of a steering system. Overall, all the choices in modeling led to expected results. The results for each method are summarized below:

- Model B can reduce backdriving depending on the simulation. It generates large currents and harsh peaks in the power when used in a feedback loop. This method produces results that can differ substantially from other models.
- Model C is prone to chattering which can lead to long simulation times depending on the value for I_{high}. However it does help reduce backdriving in all simulations.
- Model D seems to have good results with no additional parameters needed to tune. It also suffers from chattering in the step input response with the vehicle which can slow simulation time.
- Model E requires additional parameters and additional equations to implement properly. The power and current drawn in a feedback loop are larger than the other models because of the efficiency inherent in the gear modeling.
- Although Model F does not allow any communication of power between the motor and rack, given the nature of the application it does not differ too much from other methods that model the non-backdriving behavior better.

For testing with a steering control system, Models C and D seem to be good starting points as they are simple to implement. Although model E has higher fidelity, the implementation takes extra work that may not impact the overall simulation as a whole if the effect that one is after is non-backdriving. The Karnopp friction method of applying Coulomb friction can be time consuming to derive.

In this investigation, the effect of backdriving does not seem to be as large of a problem. The current the motor provides in order to perform the different maneuvers on the vehicle seems to not deviate

too much between Models C, D, and F. The small amount of power indicates that model F can be adequate to use for the simulation conditions.

Future work into this topic using vehicles would investigate disturbances into the system where random loading can propagate through the rack back to the motor, such as random wind disturbances. Disturbances and loading changes while the vehicle is steering should show more deviation of the models from Model F.

Additionally, alternative applications can be investigated where backdriving would have a bigger impact. One thought would be a velocity control instead of a position control problem. If disturbances added loading which propagates back to the motor, then that would be an application where using just a source flow would not be good enough. This would allow the forces to propagate back to the motor while the power remains positive, and the current would vary.

REFERENCES

Cheng, P.-J., and H.-P. Huang. 2011, December. "Modeling and control of the CCEA robotic arm". In *2011 IEEE International Conference on Robotics and Biomimetics*, pp. 1171–1176. Karon Beach, Thailand, IEEE.

Karnopp, D. 1985, March. "Computer Simulation of Stick-Slip Friction in Mechanical Dynamic Systems". *Journal of Dynamic Systems, Measurement, and Control* vol. 107 (1), pp. 100–103.

Loyola, J., and D. Margolis. 2021, May. "Variable wheelbase reference for vehicle with active front and rear-wheel steering". *Vehicle System Dynamics*, pp. 1–17.

Timothy Burke 2000. "Modeling and Evaluation of Nonbackdrivable Transmissions for Variable Stiffness Prostheses". Master's thesis, Carleton University, Ottawa, Ontario.

AUTHOR BIOGRAPHIES

JONATHAN LOYOLA is a Ph.D. candidate and a graduate student researcher working at the Hyundai Center of Excellence in Vehicle Dynamic Systems & Control located at the University of California, Davis. He holds a master's degree from Davis in mechanical engineering. His research interests lie in system modeling, vehicle dynamics, and controls. His email address is jonloyola@ucdavis.edu.

KYUNGBOK LEE is a senior research engineer in the Steering Engineering Design Team at Hyundai Motor Company. His primary job in Hyundai is the design of steering systems such as: electric power steering, rear-wheel steering system, and steer-by-wire systems. His email address is kblee0606@hyundai.com.

DONALD L. MARGOLIS is a professor of mechanical engineering and director of the Hyundai Center of Excellence in Vehicle Dynamic Systems & Control at UC Davis. He has extensive experience in teaching system dynamics at the graduate and undergraduate levels, consultation in vibration controls, and has published numerous papers on the industrial applications of the dynamics. His email is dlmargolis@ucdavis.edu.